ADVANCED THEORY AND SIMULATIONS
www.advtheorysimul.com

Density Functional Theory Study on the Impact of External Magnetic Fields on the Photocatalytic Properties of Metal-Doped Titanium Dioxide

Pengsheng Liu and Xiaoan Mao*

Home-made pure TiO_2, Fe/TiO_2, Co/TiO_2, Cr/TiO_2, Cu/TiO_2 and Mn/TiO_2 were tested for methylene blue degradation under UV light with a 0.1 T magnetic field (MF). Fe/TiO_2 showed the greatest improvement, with moderate effects for pure, Cu- and Mn-doped samples, while Co- and Cr-doping reduced degradation. Mechanisms were explored using DFT+U (PBE functional, VASP code) computation. DOS patterns indicates noticeable spin polarization as transition metals are doped into lattice and various degrees of bandgap decrease and the introduction of new bands within the bandgap region. The charge density patterns indicated that the doped transition metals can form new recombination centers to inhibit the electron and hole recombination. Optical properties simulations estimated photocatalytic performance through dielectric function, Cu/TiO_2 stands out with the highest dielectric constant, suggesting its superior potential for light absorption. According to the spin density results, Cu/TiO_2, Fe/TiO_2, and Mn/TiO_2 showed the highest potential of being affected by an external magnetic field, consistent with the experimental findings of enhanced photo degradation in the presence of an external MF. This research aims to elucidate the mechanisms of the external magnetic field effect on photocatalysis at the electron level.

1. Introduction

In recent years, titanium dioxide (TiO_2) has attracted significant attention due to its chemical and optical properties, as well as its potential applications in photocatalysis.[1–5] However, the inherent limitation in its bandgap has prompted researchers to explore alternative methods to enhance the photocatalytic efficiency of TiO_2. An emerging and distinctive avenue of investigation involves the application of external physical fields. While thermal,[6] electric,[7] and microwave[8] fields have been extensively researched and comprehensively understood, the study of magnetic field lags behind, with certain mechanisms and reactions remaining unclear. Further investigation is required to elucidate the full scope of the impact of external magnetic fields on photocatalysis and to unlock their untapped potential in enhancing photocatalytic processes. Although some search results may not be fully aligned with this research area, the statistics still show that research on magnetic field-photocatalysis coupling is still in its early stages but has been attracting more attention in recent years. In the published reviews,[6,9–11] the sections concerning the application of an external magnetic field on photocatalysis provide valuable insights by presenting existing research cases and perspectives. Although these reviews offer relatively comprehensive understanding on photo-magnetic coupling, a significant gap remains in elucidating the underlying reaction mechanisms. At present, the proposed explanations for the influence of an external magnetic field are primarily based on the Lorentz force and spin polarization. However, further in-depth studies are still required to establish a more direct and convincing link between experimental observations and the fundamental mechanisms.

The existing relevant researches designed based on Lorentz force and spin polarization will be reviewed. This approach is grounded in the understanding that magnetic fields can change the motion of charged particles within the magnetic field. Gao et al. applied permanent magnets beneath the photocatalytic reactor and used TiO_2 nanobelts as the photocatalyst to degrade methyl orange.[12] The photocatalytic degradation of methyl orange in the presence of magnetic field increased by 26% compared to the removal rate in the absence of external magnetic field. Gao et al. attributed this development to the Lorentz force, which can effectively separate photo-generated electrons and holes, thereby inhibiting the recombination of electrons and holes. Okumura et al. employed a similar reactor setup with Gao et al. to investigate the external magnetic field effect on the ZnO photocatalytic degradation of methylene blue.[13] The MB concentration decreased more rapidly under 0.7T magnetic field compared to that without a magnetic field. Furthermore, their finding suggested that the magnetic field effect is related to dissolved oxygen (DO) level, which can affect the formation of DO-dye complex, modify powder absorption layer and change the scavenging rate of excited electrons. Additionally, they proposed

P. Liu, X. Mao
School of Chemical and Process Engineering
University of Leeds
Woodhouse Lane, Leeds LS2 9JT, UK
E-mail: pmpl@leeds.ac.uk

The ORCID identification number(s) for the author(s) of this article can be found under https://doi.org/10.1002/adts.202501174

DOI: 10.1002/adts.202501174

an oxygen-acceleration-near-surface(OANS) model to describe the appearance of net Lorentz force on DO with paramagnetism. Numerous similar studies[14–17] have also applied permanent magnets into photocatalytic reactions and found an enhancement in photocatalytic performance in the presence of external magnetic field. Additionally, some studies explain the external magnetic field effect by spin polarization phenomenon. Spin is the intrinsic angular momentum of electrons, and spin polarization denote the alignment degree of spin orientations along a specified direction.[18] Some researchers propose that the external magnetic field can enhance the spin polarization, as the magnetic field can compel the alignment of spin orientations toward a specific orientation so that the recombination of electrons and holes can be inhibited and photocatalytic performance can be developed. For instance, Li et al. conducted a study involving the modification of TiO_2 and introduced a magnetic field into the photocatalytic reaction. They demonstrated the external magnetic field can manipulate the spin polarization of TiO_2.[19]

Currently, there is a limited number of research investigating the influence of magnetic fields on photocatalysis. In light of this research state, our study delves deeply into the potential and mechanisms of the magnetic field effect on spin polarization. Due to the limitation of current experimental technology, the first principle calculation was used to study the electron properties of TiO_2 and transition metal doped TiO_2, such as density of state, charge density, and spin density. By presenting degradation experimental observations in the presence of an external magnetic field and theoretical analyses, our study aims to contribute valuable insights to the understanding of photo-magnetic coupling. We provide rigorous degradation experimental results of photo-magnetic coupling and establish a strong connection between experimental findings and theory, offering a comprehensive examination of the role played by spin polarization in photocatalytic reactions.

2. Experimental Methods and Computational Details

This study uses 0.5at.% doping concentration Fe/TiO_2, Cu/TiO_2, Mn/TiO_2, pure TiO_2, Cr/TiO_2 and Co/TiO_2 as the photocatalyst. These catalysts were synthesized using the sol-gel method, resulting in nanoparticles with particle sizes of approximately 10–20 nm. The evaluation of the magnetic field effect was demonstrated through the photocatalytic degradation of methylene blue. By comparing the %degradation of methylene blue under light irradiation with and without the external magnetic field, the presence of the magnetic field effect was assessed. The initial methylene blue concentration was 10 mgL^{-1}. The photo-excitation of the catalysts was provided by a UV light source of the wavelength centered around 365 nm. The concentration of MB in the aqueous solution was determined using a UV spectrophotometer (PerkinElmer® Lambda XLS) by measuring the absorbance at 668 nm. In each test, one of the nano-sized materials was dispersed into the aqueous solution of MB at a loading of 1 gL^{-1}. The suspension was stirred in the dark for a duration of 30 min to reach the absorption equilibrium. Subsequently, the suspension was subjected to the UV radiation to initiate the photo-degradation reaction in a photo-reactor. A sample of the suspension was extracted to determine the concentration of methylene blue every 10 min. The sample was centrifuged for 10 min, to separate the nanoparticles from the solution.

The supercell models for transition metal doped TiO_2 were derived from the anatase unit cell, which was tetragonal structure ($I4_1/amd$). The choice of model dimensions for calculation depends on the specific doping concentrations. In this research, the doping concentration was 0.5at.% so that the computational model size was $6 \times 5 \times 1$ based on anatase unit cell. These models consisted of a total of 700 atoms, which either 185 Ti atoms or 185 Ti atoms along with one doping metal atom, and 515 oxygen atoms.

The ab initio calculation was carried out using the projector augmented wave (PAW)[20] pseudopotential method and executed with the VASP[21–24] code. The exchange-correlation energy was calculated by Perdew-Burke-Ernzerhof (PBE)[25] functional along with the GGA+U method. In this calculation the cutoff energy of the basis set was set to 520 eV. The k-points grid was chosen in the gamma scheme to achieve a precision of 0.04. The electronic self-consistent loop convergence to 1E-6eV and the ionic relaxation loop convergence criterion was set to −1E-2eV. The force on atom was required to smaller than 0.05eVnm^{-1}. The U-values[26–29] for Ti3d, O2p, Cr3d, Cu3d, Fe3d, Co3d, and Mn3d were 4, 0, 3.7, 4, 5.3, 3.32, and 3.9 respectively. These values were determined using a semi-empirical approach, in which the calculated properties were compared against corresponding experimental data. Geometry optimization, self consistent field calculations, band structure, optical properties, and spin state analysis were performed using the aforementioned conditions.

3. Photo-Magnetic Coupling Degradation

The effect of the magnetic field on photocatalytic degradation is assessed by experiments measuring the %degradation of methylene blue (MB) in the presence or absence of 0.1T external magnetic field. The detailed degradation results are displayed in **Figure 1** and **Table 1**. Fe/TiO_2 exhibits the best photocatalytic performance among these six catalysts. The magnetic field has a significant effect on the photocatalytic performance of Fe/TiO_2, resulting in an approximate 6.1% increase in methylene blue removal and a rise of 0.0393 in the kinetic rate constant. Cu/TiO_2, Mn/TiO_2, and pure TiO_2 are the second performance. While Cu/TiO_2, Mn/TiO_2, and pure TiO_2 exhibit a development on photocatalytic and photo-magnetic performance. For Cu/TiO_2, Mn/TiO_2, and pure TiO_2, the magnetic field also enhances photocatalytic performance, with MB removal of approximately 6.9%, 6.6%, and 7.5%, and corresponding rises in kinetic rate constants of 0.0181, 0.0172, and 0.0129, respectively. Although the increase in methylene blue removal for Fe/TiO_2 is less pronounced than that of Cu/TiO_2, Mn/TiO_2, and pure TiO_2, it is noteworthy that under the influence of a 0.1 T external magnetic field, the degradation reaction nearly reaches complete removal, and the enhancement in reaction rate is significantly greater than that of the other materials. The magnetic field effect is also observed on Cu/TiO_2, Mn/TiO_2, and pure TiO_2, with the effect being more pronounced on Cu/TiO_2, Mn/TiO_2, compared to pure TiO_2. Which is differ-

Table 1. Methylene blue degradation and kinetic rate constants in 60 min for methylene blue photo-degradation with and without a 0.1 T external magnetic field.

Catalyst	MB Degradation(%)		Kinetic Constant(k(min^{-1}))	
	0.1 T magnetic field	No magnetic field	0.1 T magnetic field	no magnetic field
pure TiO_2	90.1%	82.6%	0.05	0.0371
Fe^{3+}/TiO_2	99.3%	93.2%	0.0956	0.0563
Cu^{2+}/TiO_2	94.8%	87.9%	0.0621	0.044
Mn^{2+}/TiO_2	93.9%	87.3%	0.0597	0.0425
Cr^{3+}/TiO_2	74.2%	74.5%	0.0271	0.0276
Co^{2+}/TiO_2	82.1%	82.7%	0.0347	0.0350

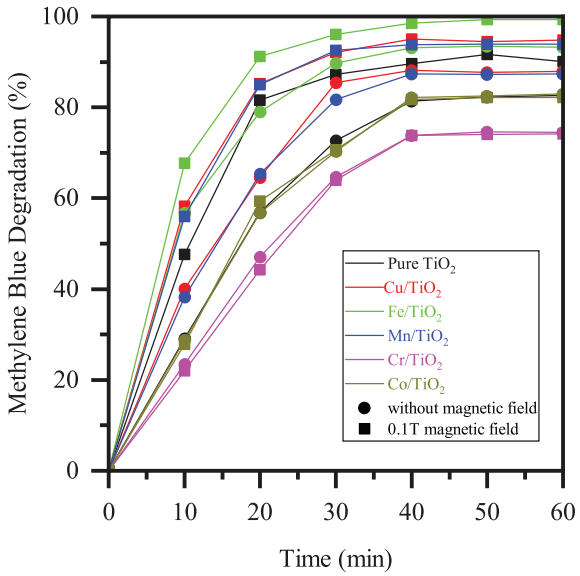

Figure 1. Photocatalytic degradation of methylene blue in the presence and absence of 0.1T external magnetic field.

ent from the above results, Cr/TiO_2 and Co/TiO_2 do not show any improvement when the 0.1T external magnetic field is applied. In conclusion, the magnetic field effect on the photocatalytic performance of above six catalysts can be ranked as follows: Fe/TiO_2 > Cu/TiO_2 and Mn/TiO_2 > pure TiO_2. Notably, for Co/TiO_2 and Cr/TiO_2, the external magnetic field was found to have little effect on their photocatalytic performance.

In the photocatalytic degradation experiments, the magnetic field effect was observed. Interestingly, the magnetic field exhibited different effects on different catalysts, with some showing a significant improvement in photocatalytic degradation and others showing little impact. To investigate this phenomenon, this study employed DFT simulations to examine the band structure, density of states, spin, and charge density, and optical properties of six catalysts. This approach attempts to link the experimental findings with spin polarization theory, providing strong data to support the theory that spin polarization is the underlying mechanism of the magnetic field effect, rather than merely proposing an explanatory hypothesis.

Table 2. Crystal parameters (*a*, *b* and *c*) of 0.5at% (pure, Co, Cr, Cu, Fe, and Mn) doped TiO_2.

Doping concentration	Catalyst	*a*	*b*	*c*	Magnetization(μB)
6 × 5 × 1(0.54at%)	anatase	3.8576	3.8574	9.7412	0
	Co/TiO_2	3.8559	3.8575	9.7288	−0.973
	Cr/TiO_2	3.8559	3.8590	9.7331	1.995
	Cu/TiO_2	3.8576	3.8572	9.7279	2.625
	Fe/TiO_2	3.8575	3.8572	9.7284	1.935
	Mn/TiO_2	3.8569	3.8570	9.7322	0.967

4. Computational Results and Discussion

4.1. Structural Optimization

First of all, geometry optimization calculations were performed to obtain the lowest energy structure. The computational results for the crystal parameters *a*, *b*, *c* and magnetic moment are listed in the **Table 2**. The crystal parameter of anatase unit cell is $a \times b \times c = 3.7784 \times 3.7784 \times 9.5143$. The lattice parameters of transition metal doped anatase models show minimal variation when compared to the lattice parameter of undoped anatase along the *a* and *b* directions, with changes on the order of 10^{-5} to 10^{-4}, which can be safely disregarded. In terms of the *c* direction, a noticeable change is observed, which can be primarily attributed to the limited thickness of the supercell along this orientation. As a result, the lattice along the *c* direction is more susceptible to alterations when transition metals doping. In the case of a bulk of transition metals doped anatase, the lattice parameter *c* tends to be similar to *a* and *b*, these lattice parameters do not undergo significant changes compared to pure anatase. Thus, transition metals do not significantly impact the lattice parameters of doped TiO_2.

The **Figure 2** illustrates the charge density distribution around Ti, O, and transition metal atoms. The charge density provides insight into the distribution of electrons surrounding the atoms. In the case of pure TiO_2, the charge density around both Ti and O atoms is precisely identical. However, when considering doped transition metals in TiO_2, there is a notable increase in the charge density around Co, Cu, Fe, and Mn atoms. This suggests that these doped atoms attract electrons from the surrounding O atoms, resulting in a strengthened charge density. This phenomenon indicates that doped transition metals pull the electrons closer to themselves,[30] transforming into recombination

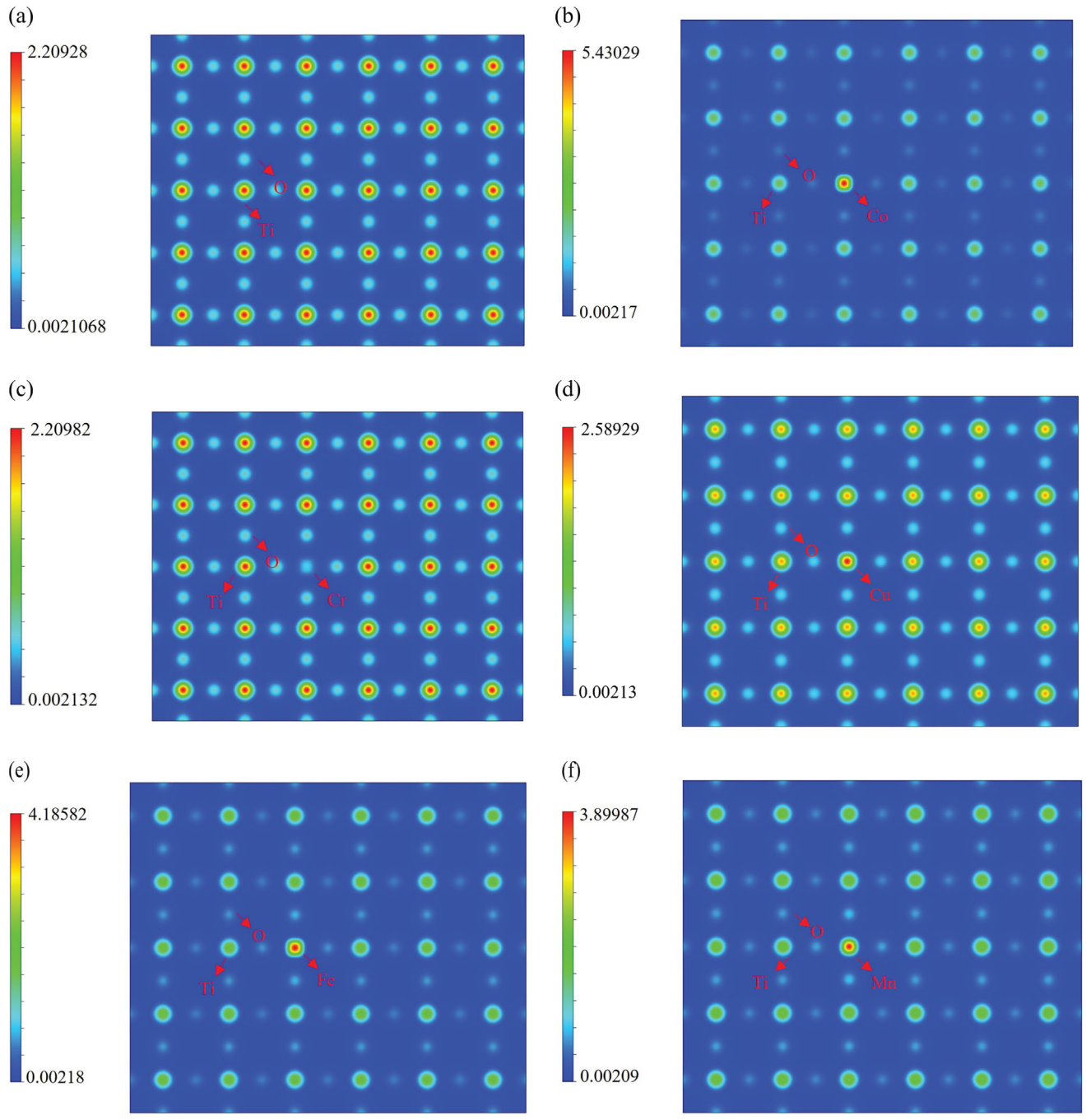

Figure 2. Charge density patterns of 0.5at.% a) pure TiO_2, b) Co/TiO_2, c) Cr/pure TiO_2, d) Cu/pure TiO_2, e) Fe/pure TiO_2, and f) Mn/pure TiO_2.

centers that hinder the recombination of electrons and holes.[31] Hence, controlling the doping concentration becomes a critical factor. In contrast, the charge density around Cr significantly decreases, suggesting that the overall charge surrounding the Cr atom is balanced and cancels out. Despite the reduction in charge density, this characteristic promotes the diffusion of electrons.[31] In summary, the variations in charge density provide valuable insights into the electronic behavior of doped transition metals in TiO_2. Understanding these patterns is crucial for optimizing material properties, particularly in applications where electron diffusion and recombination processes play a significant role.

4.2. Electronic Structure

To investigate the electronic structure, the band structure and density of state(DOS) were performed after geometry optimization and self-consistent field calculations. It is worth noting that the calculated value of bandgap is significantly underestimated

than experimental value (E_g = 3.2eV), this is due to the PBE functional used in this research. The PBE functional does not include exchange correlation potential, even though DFT+U method introduce parameter U to adjust the Ti3d, O2p, and transition metal 3d orbitals, but the estimated bandgap is still lower than experimental results. It is important to emphasize that the U value cannot be increased in order to match the 3.2 eV bandgap. This practice is fundamentally incorrect, as an excessively high U value will lead to the VBM is not associated with the Ti3d orbital. For transition metals, the appropriate range for U value generally falls 2 to 4 eV. The choice of U value is commonly base on semi-empirical or Cococcioni's method.[32] Despite the energy underestimation, it is important to emphasize that discussions concerning the energy gap remain valid. Our discussions primarily focus on relative energy changes rather than absolute values.

The total density of states (TDOS) is presented in **Figure 3**. For consistency, the Fermi energy of all models was set to 0 eV when plotting the TDOS. Examining the density of states at 0 eV, all catalysts exhibit semiconductor properties. Specifically, anatase, Cr/TiO_2, Cu/TiO_2, and Mn/TiO_2 show no electron occupancy at this energy level.[33] In contrast, Co/TiO_2 and Fe/TiO_2 also remain semiconductors, despite the presence of some electronic states at the Fermi level. These states originate from doping. Second, we will delve into the study of bandwidth and energy levels. In all the TDOS of transition metal doped TiO_2, it is evident that new energy levels appear between valence band maximum(VBM) and conduct band minimum(CBM), these newly introduced bands play a crucial role in reducing the energy required for electron excitation, thereby expand the optical absorption spectrum. Electrons can be excited to these intermediate bands and then subsequently promoted to the conduct band by visible light or lower energy.[34,35] Consequently, from a theoretical perspective, the method of transition metal doping proves to be highly advantageous for enhancing the photocatalytic performance of anatase. As shown in Figure 3, the calculated bandgaps for various TiO_2 configurations consistently measure approximately 2.41 eV. But the difference is the relative positions of the valence band maximum and conduction band minimum. In the case of anatase, Cu/TiO_2 and Mn/TiO_2, the positions of the VBM and CBM remain unchanged even after the copper and manganese atoms are doped into TiO_2, indicating that Cu and Mn atoms mainly introduce impurity energy levels (IELs) within the anatase band structure, leading to a narrowing the band gap of TiO_2. In the instances of Co/TiO_2, Cr/TiO_2 and Fe/TiO_2, the overall energies of the conduction band and valence band exhibit a decrease by 0.17, 0.28, and 0.84 eV respectively, but the energy gap between them remains consistent. This phenomenon can be attributed to either a reduction in the super cell symmetry resulting from significant electronic non-locality[36] or the 3d orbital of metal atoms hybridization with O2p or Ti3d.[37] Next, the DOS for both spin up and spin down state will be discussed. For pure TiO_2, the electronic states for spin up and spin down are identical, resulting in no observation of spin polarization. However, when we shift our focus to modified TiO_2, the transition metals not only introduce IELs into the bandgap but also change the spin state. The changes manifest in the valence band, conduction band and bandgap. Specifically, new energy levels within the bandgap have distinct spin states at the same energy, giving rise

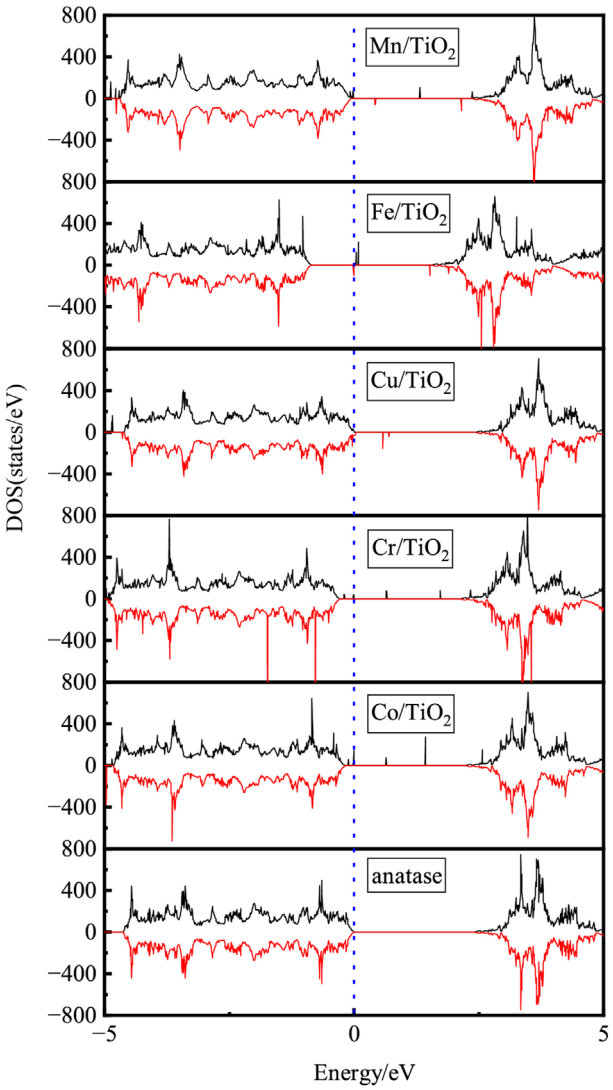

Figure 3. Total density of state of anatase with transition metal doping (Co, Cr, Cu, Fe, and Mn) in 0.5at.% doping concentration.

to spin polarization. This spin polarization arises due to the presence of doped transition metals. Additionally, the transition metals affect the spin state of O atoms and Ti atoms. The introduction of transition metals will lead to alterations in the spin states, due to hybridization between the metal atoms and O and Ti atoms.[38] Furthermore, it is worth noting that spin polarization can affect the catalysts' performance in the presence of an external magnetic field.[39]

The band structure patterns are shown in **Figure 4**, which align with DOS results, the bandgap of TiO_2 remains approximately the same, with shift toward smaller values. In the figure, the region between the two red dotted lines represents the TiO_2 bandgap. In the band structure of anatase, no bands exist within this specific region. However, in the case of transition metal doped TiO_2, it is obviously that the introduction of one or more energy levels by transition metals falls within the TiO_2 bandgap

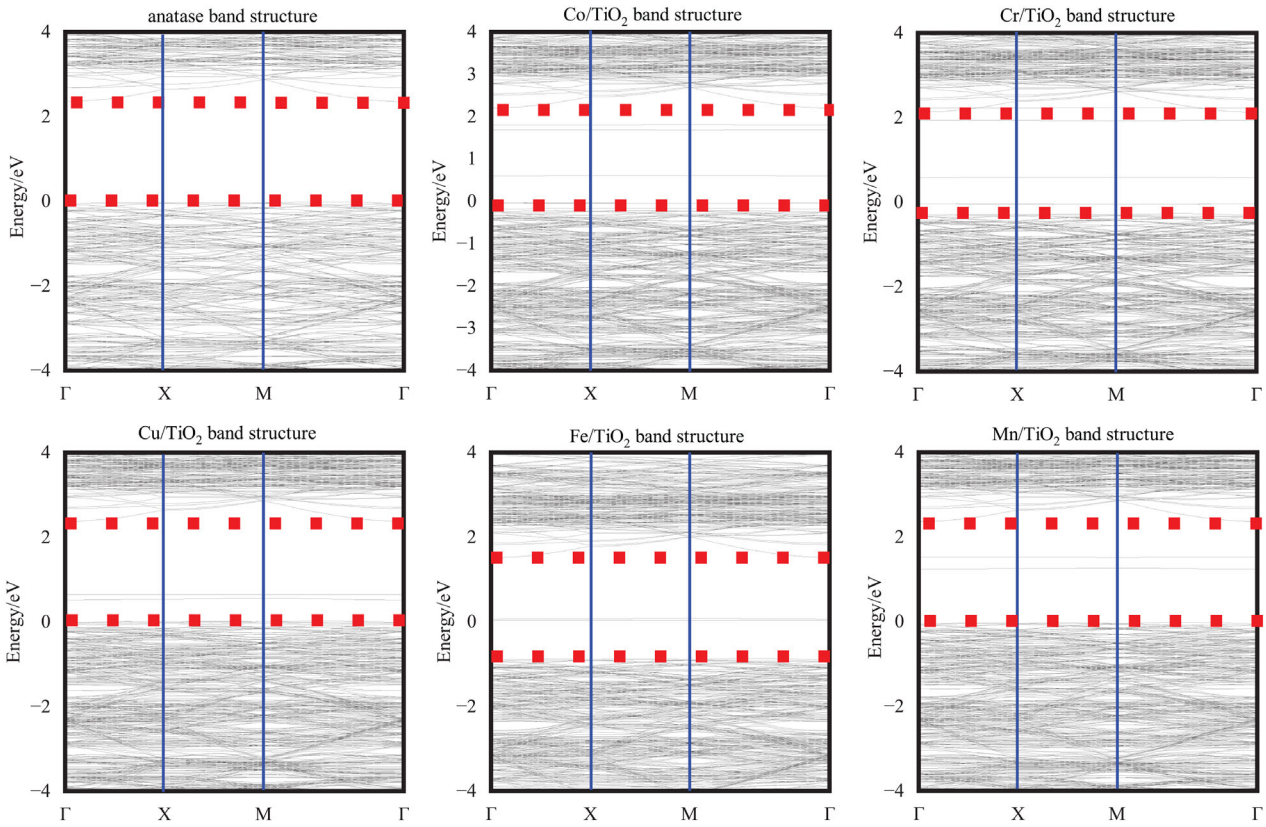

Figure 4. Band structure of anatase and transition metals (Co, Cr, Cu, Fe, and Mn) doped TiO_2.

so that doped TiO_2 catalysts can be excited by lower energy or visible light.

4.3. Optical Properties

The optical properties will be elucidated through the dielectric function and absorption coefficient, which are derived from the effect of incident light with the photocatalysts' models for the geometry-optimized models. The dielectric function is expressed as:

$$\varepsilon(\omega) = \varepsilon_1(\omega) + i\varepsilon_2(\omega) \quad (1)$$

where $\varepsilon_1(\omega)$ is the real part and $\varepsilon_2(\omega)$ is the imaginary part. The real part is referred to as electronic polarizability or refractive index and the imaginary part is associated with the absorption energy with electromagnetic radiation and electronic absorption of materials.[40]

Figure 5 presents the real and imaginary parts of dielectric function. The intercept of the real part corresponds to the dielectric constant $\varepsilon_1(0)$. $\varepsilon(0)$ is inversely related to the bandgap(E_g).[41] The values of $\varepsilon_1(0)$ for Cu/TiO_2, Mn/TiO_2, Cr/TiO_2, Co/TiO_2, Fe/TiO_2, and TiO_2 are 7.3817, 6.4208, 6.5938, 6.3817, 6.27, and 6.0947 respectively in descending order. Based on these data, Cu/TiO_2 may exhibit superior photocatalytic properties compared to the other catalysts. The positions of the highest peaks are approximately centered around 3 eV, with slight shifts depending on the specific doping elements. In Figure 5b, the imaginary part is presented, the positions of peaks are located at around 4.2 eV. Fe/TiO_2 exhibits a notable difference from other catalysts. While the highest peak position remains exactly the same in the imaginary curves, the value of $\varepsilon_2(\omega)$ decreases as the energy increases. Despite repeated calculations to check for potential errors, the results still remain consistent. Factors contributing to this phenomenon may be attributed to the selection of the U value, the use of the PBE functional and the possibility of sub-optimal geometry optimization resulting from the large model size.

The dielectric constant plays a role in photocatalysis, which involves the utilization of light in chemical reactions. The dielectric constant serves as an indicator of the photocatalyst's ability to absorb and interact with incident light, as well as the capabilities of separation and mobility of photo-generated charge carriers. Among the six photocatalysts, Cu/TiO_2 stands out with the highest dielectric constant, suggesting that Cu/TiO_2 has the greatest potential for light absorption and enhancing electron-hole separation and reducing charge recombination.[42] And pure anatase exhibits the lowest dielectric constant, which indicates that the transition metal doping method indeed improve the light absorption and charge separation abilities.

4.4. Spin Density

In this section, the spin density will be discussed with the hope of identifying whether the magnetic field effect on photocatalytic

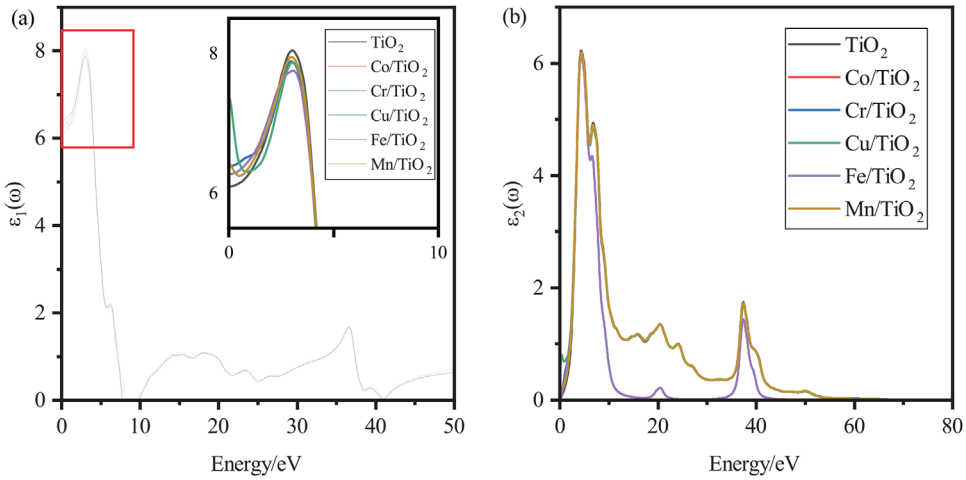

Figure 5. a) Real part of dielectric function. b) Imaginary part of dielectric function.

reaction can be attributed to spin polarization or any other spin related factors. **Figure 6** illustrates the spin density distribution. There is no spin distribution observed around the Ti and O atoms, so the anatase model and spare atoms in the doping models are not displayed. In the figures, the yellow color surrounding the atoms represents the spin-up state, while the green color represents the spin-down state.

First, when transition metals are doped into TiO_2 crystal lattice, spin polarization is introduced into the structures. The spin polarization manifests on the doped metal atoms and the first nearest neighboring O atoms. Notably, in the case of Cu/TiO_2, the spin state distribution extends to the second nearest neighboring oxygen atoms, indicating that the magnetic orbital coupling extends to more distant atoms and effectively forming a magnetic field percolation effect.[43] Based on the results of spin distribution and the magnetization data presented in Table 2, it can be confidently concluded that spin polarization indeed occurs in the transition metal-doped TiO_2 samples.

Second, the spin density patterns will be studied. According to the shape of spin density, these five models can be categorized into three groups (Co/TiO_2 and Mn/TiO_2, Cr/TiO_2, and Fe/TiO_2, Cu/TiO_2). In the case of Co/TiO_2 and Mn/TiO_2, the spin density shape of these two models is d-orbital shape. The d orbital shape is commonly observed in complexes with $t_{2g}^6 e_g^3$ configuration. There are positive spin density regions around the Co and Mn positions, which is an expected outcome due to the interaction between the metal and oxygen contributions within the e_g molecular orbitals.[44,45] The spin density shape of Cr/TiO_2 and Fe/TiO_2 is different from Co/TiO_2 and Mn/TiO_2, which are similar to d orbital shape. Instead, the spin density patterns exhibit a shape that approximates a cube, this shape is associated with $t_{2g}^3 e_g^4$ configuration and is influenced by the presence of a significant spin component along the metal-O directions introduced by the polarization functions utilized in the calculations.[45] In the case of Cu doped TiO_2 model, the spin density shape is different from the previously mentioned two shapes. This disparity arises due to partial occupancy in the e orbitals (e_g). This specific shape can be readily understood as a combination of the shapes of two e_g orbitals, each having lobe in the direction of the six ligands.[46]

In the preceding paragraph, we discussed the spin density shapes to gain a fundamental understanding of spin density. In the following section, we will delve into the discussion of spin states and their relationship to magnetization and magnetic field effect. For pure TiO_2, the spin density is zero for all atoms on all orientations. In the case of Co/TiO_2, the net spin state is observed to be spin down, whereas, for the other models, the net spin density is spin up. Across all five models, it's noteworthy that the spin polarization is localized on the doped metal atoms and oxygen atoms, with no apparent relationship to the Ti atom. This result suggests that the spin polarization is primarily attributed to the hybridization between the oxygen 2p orbital and the metal 3d orbital. The order of spin polarization is $Cu/TiO_2 > Cr/TiO_2 \approx Fe/TiO_2 > Mn/TiO_2 \approx Co/TiO_2$.

As shown in Table 2, Cu/TiO_2, Fe/TiO_2, Cr/TiO_2, and Mn/TiO_2 all exhibit positive non-zero total magnetization, indicating the presence of magnetic moments and potentially magnetic ordering, suggesting ferromagnetic or ferrimagnetic behavior.[47] In the case of Co/TiO_2, the negative, non-zero magnetization implies that the direction of the magnetization vector, relative to a chosen reference, is indicative of ferrimagnetic behavior.[47] Analysis of the VASP output reveals that the magnetic moment alignments of individual electrons in these catalysts display both positive and negative orientations, with varying magnitudes. This observation supports the conclusion that these catalysts likely exhibit characteristics consistent with ferrimagnetism. This magnetization is typically lower than that observed in ferromagnetic materials. When materials exhibit ferrimagnetic properties, they tend to be responsive to external magnetic fields, resulting in a spin polarization. However, in the case of pure TiO_2, the impact of external magnetic fields on spin polarization may be comparatively limited. In the context of photocatalysis, it is important to explore the interaction between spin polarization effects and the influence of an external magnetic field. Spin polarized electrons play a significant role in reducing electron-hole recombi-

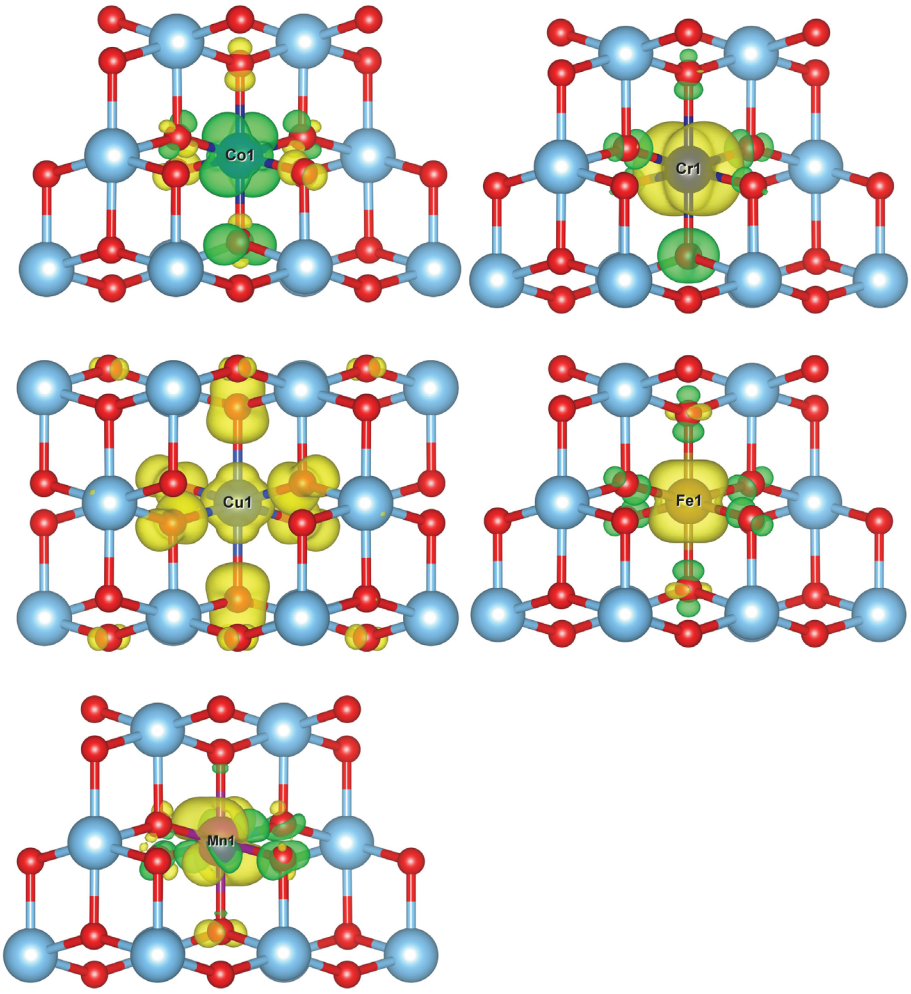

Figure 6. Spin density distribution of Co, Cr, Cu, Fe, and Mn doped TiO_2.

nation during the charge transfer process.[48] When photocatalysts are excited, the excited electrons transition to the conduction band, leaving holes with the same spin state in the valence band. However, the application of an external magnetic field introduces additional effects, such as spin-orbital coupling and hyperfine interactions.[49] These effects can alter the original spin direction of excited electrons. Consequently, recombination is inhibited due to the lack of electrons and holes with matching spin states.[50,51] Moreover, the external magnetic field can prolong the preservation of the spin state, in materials exhibiting ferrimagnetic properties. This means that pure TiO_2 is less affected by external magnetic field because of its zero magnetization.

In conclusion, based solely on the analysis of spin density distribution, the photocatalytic performance of Cu/TiO_2 is likely to be the most significantly affected by the external magnetic field. Following this, the materials Cr/TiO_2 and Fe/TiO_2 are expected to be moderately affected. In contrast, Mn/TiO_2 and Co/TiO_2 may experience a relatively lower effect from external magnetic fields. As for pure TiO_2, it appears to be inherently unresponsive to the magnetic field effect.

5. Conclusion

In this research, photo-magnetic coupling MB degradation experiment results and first principle calculation results by using 0.5at.% (pure, Co, Cr, Cu, Fe, and Mn) doped TiO_2 as samples were displayed. In a practical situation, the rank of sensitivity to external magnetic field among these six catalysts is as follow: Fe/TiO_2 > Cu/TiO_2 and Mn/TiO_2 > pure TiO_2 > Co/TiO_2 and Cr/TiO_2. Specifically, 0.5at.% Fe-doped TiO_2 show the most response to the 0.1T external magnetic field, while Co/TiO_2 and Cr/TiO_2 display no response to the 0.1T external magnetic field. Upon observing these results, DFT simulation was employed to characterize the electron structure, band structure, dielectric constant, and spin polarization of these catalysts to study the external magnetic field effect on electrons and spin state so that the connection between practical experiment and spin polarization theory can be established. The models utilized in these calculations are quite different from other researches, the doping concentration of the models are 0.5at.%, which is same as the doping concentration of real catalysts. The models developed in this

research make a substantial contribution to photocatalytic simulation and the study of photo-magnetic coupling. The distinctive feature is the big volume, signifying a substantial computational demand. This calculation, while requiring heavy computational resources, enhances the realism and accuracy of the simulations, providing valuable insights into the relationship between catalyst composition, external magnetic fields, and the resulting photocatalytic performance.

The calculation results suggest that the external magnetic field has a notable effect on Cu/TiO_2 compared to other samples. This conclusion is drawn from the favorable dielectric constant, spin density pattern, and magnetization. Further analysis of the band structure and density of states indicates that Cu-doped TiO_2 has potential for the development of photocatalytic performance. However, due to the zero total spin density of pure TiO_2, there is reason to doubt that pure TiO_2 would not be affected by an external magnetic field to induce spin polarization. The similarities observed between Fe/TiO_2 and Cr/TiO_2 in the calculation results suggest that they should respond to external magnetic fields in a similar behavior. Mn/TiO_2 and Co/TiO_2 are also expected to be affected to some extent. Combining these computational results, a hypothesis regarding the rank of catalysts' response to the 0.1 T external magnetic field can be proposed as follows: Cu/TiO_2 > Fe/TiO_2 and Cr/TiO_2 > Mn/TiO_2 and Co/TiO_2.

Integrating results of practical degradation and simulation suggests that spin polarization may contribute to effect of external magnetic fields on photocatalytic performance. However, it is evident that spin polarization is just one factor among several factors influencing the performance of photocatalysts in the presence of a magnetic field. This research proposes several hypotheses to comprehensively address the potential probability. 1) magnetic field threshold: there is a magnetic field intensity threshold, implying that the intensity of magnetic field must surpass a certain level for the magnetic field effect to manifest in the photocatalytic reactions. Below this threshold, the impact on photocatalytic performance may be negligible. 2) effect on free radicals: The external magnetic field may not just affect the electron spin state of the molecule but also affect the photo-generated free radicals, such as prolong the lifetime of free radicals. 3) physical properties of catalysts: physical properties of the catalysts also play a crucial role in determining its response to the external magnetic field, such as surface properties, particle size and surface area etc.

In conclusion, 0.1 T magnetic field can develop the photocatalytic performance of Fe/TiO_2, Cu/TiO_2, Mn/TiO_2, and pure TiO_2. Conversely, Co/TiO_2 and Cr/TiO_2 exhibit no impact from external magnetic field. Spin polarization do play a crucial role in the photo-magnetic coupling but it does not represent the sole mechanism. Additional factors may collaborate with spin polarization theory to contribute to the photo-magnetic coupling effect.

Author Contributions

P.L. performed conceptualization, experimental work, computational work, writing - review, and editing, and writing - original draft. X.M. performed writing - review and editing, supervision, and conceptualization.

Conflict of Interest

The authors declare no conflict of interest.

Data Availability Statement

The data that support the findings of this study are available from the corresponding author upon reasonable request.

Keywords

DFT, magnetic field effect, photocatalysis, spin polarization, TiO_2, transition metal-doping

Received: June 17, 2025
Revised: July 29, 2025
Published online:

[1] H. Lin, C. Huang, W. Li, C. Ni, S. I. Shah, Y.-H. Tseng, *Appl. Catal., B* **2006**, *68*, 1.
[2] K. Nakata, A. Fujishima, *J. Photochem. Photobiol., C* **2012**, *13*, 169.
[3] Q. Guo, C. Zhou, Z. Ma, X. Yang, *Adv. Mater.* **2019**, *31*, 1901997.
[4] J. Schneider, M. Matsuoka, M. Takeuchi, J. Zhang, Y. Horiuchi, M. Anpo, D. W. Bahnemann, *Chem. Rev.* **2014**, *114*, 9919.
[5] A. Fujishima, X. Zhang, D. A. Tryk, *Surf. Sci. Rep.* **2008**, *63*, 515.
[6] X. Li, W. Wang, F. Dong, Z. Zhang, L. Han, X. Luo, J. Huang, Z. Feng, Z. Chen, G. Jia, T. Zhang, *ACS Catal.* **2021**, *11*, 4739.
[7] P. Alulema-Pullupaxi, P. J. Espinoza-Montero, C. Sigcha-Pallo, R. Vargas, L. Fernandez, J. M. Peralta-Hernandez, J. L. Paz, *Chemosphere* **2021**, *281*, 130821.
[8] J. Zhou, Z. You, W. Xu, Z. Su, Y. Qiu, L. Gao, C. Yin, L. Lan, *Sci. Rep.* **2019**, *9*, 5470.
[9] C. Hu, S. Tu, N. Tian, T. Ma, Y. Zhang, H. Huang, *Angew. Chem. Int. Ed.* **2021**, *60*, 16309.
[10] T. Lv, J. Li, N. Arif, L. Qi, J. Lu, Z. Ye, Y.-J. Zeng, *Matter* **2022**, *5*, 2685.
[11] Y. Zhang, Y. Tang, X. Yang, D. Feng, B. Feng, R. Guan, G. Che, *Small Methods* **2025**, *9*, 2402041.
[12] W. Gao, J. Lu, S. Zhang, X. Zhang, Z. Wang, W. Qin, J. Wang, W. Zhou, H. Liu, Y. Sang, *Adv. Sci. (Weinh)* **2019**, *6*, 1901244.
[13] H. Okumura, S. Endo, S. Joonwichien, E. Yamasue, K. Ishihara, *Catal. Today* **2015**, *258*, 634.
[14] Y. Liu, L. Shen, H. Lin, W. Yu, Y. Xu, R. Li, T. Sun, Y. He, *J. Membr. Sci.* **2020**, *612*, 118378.
[15] J. Li, Q. Pei, R. Wang, Y. Zhou, Z. Zhang, Q. Cao, D. Wang, W. Mi, Y. Du, *ACS nano* **2018**, *12*, 3351.
[16] Y. Lu, B. Ren, S. Chang, W. Mi, J. He, W. Wang, *Mater. Lett.* **2020**, *260*, 126979.
[17] N. Li, M. He, X. Lu, L. Liang, R. Li, B. Yan, G. Chen, *Sci. Total Environ.* **2021**, *761*, 143268.
[18] S. C. Ray, in *Magnetism and Spintronics in Carbon and Carbon Nanostructured Materials*, (Ed.: S. C. Ray) Micro and Nano Technologies, Elsevier, Amsterdam **2020**, pp. 1–21.
[19] L. Pan, M. Ai, C. Huang, L. Yin, X. Liu, R. Zhang, S. Wang, Z. Jiang, X. Zhang, J. J. Zou, W. Mi, *Nat. Commun.* **2020**, *11*, 418.
[20] P. E. Blöchl, *Phys. Rev. B* **1994**, *50*, 17953.
[21] G. Kresse, J. Hafner, *Phys. Rev. B* **1993**, *47*, 558.
[22] G. Kresse, J. Furthmüller, *Comput. Mater. Sci.* **1996**, *6*, 15.
[23] G. Kresse, J. Furthmüller, *Phys. Rev. B* **1996**, *54*, 11169.
[24] G. Kresse, D. Joubert, *Phys. Rev. B* **1999**, *59*, 1758.
[25] J. P. Perdew, K. Burke, M. Ernzerhof, *Phys. Rev. Lett.* **1996**, *77*, 3865.
[26] F. Zhou, M. Cococcioni, C. A. Marianetti, D. Morgan, G. Ceder, *Phys. Rev. B* **2004**, *70*, 235121.

[27] M. Cococcioni, S. De Gironcoli, *Phys. Rev. B* **2005**, *71*, 035105.
[28] L. Wang, T. Maxisch, G. Ceder, *Phys. Rev. B* **2006**, *73*, 195107.
[29] A. Jain, G. Hautier, S. P. Ong, C. J. Moore, C. C. Fischer, K. A. Persson, G. Ceder, *Phys. Rev. B* **2011**, *84*, 045115.
[30] L.-B. Mo, Y. Wang, Y. Bai, Q.-Y. Xiang, Q. Li, W.-Q. Yao, J.-O. Wang, K. Ibrahim, H.-H. Wang, C.-H. Wan, J.-L. Cao, *Sci. Rep.* **2015**, *5*, 17634.
[31] H. Usui, Y. Domi, H. Sakaguchi, *ACS Appl. Energy Mater.* **2023**, *6*, 4089.
[32] M. Cococcioni, S. De Gironcoli, *Phys. Rev. B* **2005**, *71*, 035105.
[33] K. Shum, *J. Appl. Phys.* **1991**, *69*, 6484.
[34] A. Bouaine, G. Schmerber, D. Ihiawakrim, A. Derory, *Mater. Sci. Eng., B* **2012**, *177*, 1618.
[35] D. Singh, N. Singh, S. D. Sharma, C. Kant, C. Sharma, R. Pandey, K. Saini, *J. Sol-Gel Sci. Technol.* **2011**, *58*, 269.
[36] G. Shao, *J. Phys. Chem. C* **2008**, *112*, 18677.
[37] Y. Wang, R. Zhang, J. Li, L. Li, S. Lin, *Nanoscale Res. Lett.* **2014**, *9*, 1.
[38] M. Swart, M. Gruden, *Acc. Chem. Res.* **2016**, *49*, 2690.
[39] Q. Yang, X. Tong, Z. Wang, *Mater. Rep. Energy* **2024**, *4*, 100253.
[40] A. Reshak, *Phys. Chem. Chem. Phys.* **2014**, *16*, 10558.
[41] D. R. Penn, *Phys. Rev.* **1962**, 2093.
[42] F. Hedhili, M. Gandouzi, S. M. Al-Shomar, Q. Mahmood, S. Chebaane, F. Alimi, A. Meftah, *Phys. Scr.* **2022**, *97*, 065818.
[43] Z. Tan, L. Wang, Y. Yang, W. Xiao, *Eur. Phys. J. B* **2012**, *85*, 1.
[44] R. F. Bader, *Acc. Chem. Res.* **1985**, *18*, 9.
[45] E. Ruiz, J. Cirera, S. Alvarez, *Coord. Chem. Rev.* **2005**, *249*, 2649.
[46] C. Desplanches, E. Ruiz, A. Rodríguez-Fortea, S. Alvarez, *J. Am. Chem. Soc.* **2002**, *124*, 5197.
[47] G. Florio, in *Encyclopedia of Smart Materials*, (Ed.: A.-G. Olabi), Elsevier, Oxford **2022**, pp. 1–9.
[48] L. Pan, M. Ai, C. Huang, L. Yin, X. Liu, R. Zhang, S. Wang, Z. Jiang, X. Zhang, J.-J. Zou, W. Mi, *Nat. Commun.* **2020**, *11*, 418.
[49] F. Schwabl, *Quantum mechanics*, Springer Science & Business Media, Berlin **2007**.
[50] M. N. Baibich, J. M. Broto, A. Fert, F. N. Van Dau, F. Petroff, P. Etienne, G. Creuzet, A. Friederich, J. Chazelas, *Phys. Rev. Lett.* **1988**, *61*, 2472.
[51] J. Li, Q. Pei, R. Wang, Y. Zhou, Z. Zhang, Q. Cao, D. Wang, W. Mi, Y. Du, *ACS nano* **2018**, *12*, 3351.